Differentiating measuring coils for pulsed currents in the MA/MHz range

E. Boggasch[a] and R. Grüb

CERN-European Organization for Nuclear Research, 1211 Geneva, Switzerland

(Received 13 October 1986; accepted for publication 22 April 1987)

The design and construction of a high-performance differentiating pick-up coil for a 500-kA/4-μs pulsed current is described. Based on the Rogowski principle, the coil was made by using the printed-circuit technique. The coil is 1 mm thick; inclusive of electrostatic shielding and can be reproduced from one master print at nearly any size. Measurements up to 5 MHz showed no significant change of self-inductance. We believe that the coil is a versatile tool to measure and monitor current pulsed in the megampere/megahertz range.

INTRODUCTION

For the plasma lens project at CERN,[1] a pulse generator[2] was built to deliver peak current pulses up to 500 kA in a repetitive mode at 0.5 Hz into a common z-pinch load.[3] The pulse generator consists essentially of four capacitor banks which are discharged simultaneously by four high-current pseudospark switches.[4–7] The stored energy is transferred via four strip lines to the centrally located plasma lens. The main characteristics of the current generator are listed in Table I. A simplified block diagram is shown in Fig. 1.

Control of the switching delay time to achieve exact parallel discharge of the four banks, as well as examination of the plasma behavior in the lens, is essential. As the plasma load presents the main inductance of the discharge circuit, plasma dynamics resulting in pinching or instabilities can be observed by the total current signal. This requires a precise high stability current monitoring system.[8–10] The approximate equation describing the peak discharge current for the LRC current generator is given below:

$$\hat{I} = \frac{U_0}{\sqrt{\frac{L_p}{C}}\left[\sqrt{\frac{L_p + L_c}{L_p}} + \left(\frac{\pi}{4}\frac{(R_p + R_c)^2 C}{L_p}\right)\right]}, \quad (1)$$

where U_0 is the charging voltage at t_0, L_p is the inductance of the plasma, L_c is the remaining inductance, C is the capacitance of the capacitor banks, R_c is the circuit, and R_p is the plasma resistance. The energy transfer efficiency from the capacitor banks to the plasma lens can be expressed as

$$n = L_p \hat{I}^2 / C U_0^2 . \quad (2)$$

Both R_c and L_c must, therefore, be kept as low as possible to minimize ohmic losses and to reach high peak currents; R_c and L_c should, therefore, not be increased by the measuring system.[11]

This requirement excludes ohmic or inductive shunts[12,13]; measuring devices being both galvanically coupled to the circuit, and hence, requiring differential measuring at high potential. Hall-effect arrangements allow only punctual measurement at the pick-up point; the expected unsymmetrical current density in the 580-mm-wide strip lines would falsify the measurement. Other methods, such as Faraday rotation,[14] require additional equipment.

Furthermore, a locally space-distributed current density $\mathbf{j}(r,\phi)$ is expected in the plasma. Therefore, current measurement directly around the plasma volume is required. For these reasons, only pick-up coils could be used. The integrated induced voltage in such coils, created by the varying magnetic flux, represents a real image of the current.

TABLE I. Characteristics of the pulse generator.

1.	Capacitance, total	108 μF
2.	Nominal charging voltage	16 kV
3.	Maximum charging voltage	20 kV
4.	Stored energy at nominal voltage	13.8 kJ
5.	Stored energy at maximum voltage	21.6 kJ
6.	Peak discharge current at nominal voltage	400 kA
7.	Peak discharge current at maximum voltage	500 kA
8.	Inductance of plasma lens	20–100 nH
9.	Circuit inductance	10 nH
10.	Circuit impedance	9.6 mΩ
11.	Rise time to first current maximum	1.6 μs
12.	Equivalent half nt half-sine-wave length	7.4 μs
13.	Initial dI/dt at nominal current	6×10^{11} A s^{-1}
14.	Voltage reversal	~45%
15.	Strip line cross section	540×11 mm
16.	Distance between conductors	0.9 mm
17.	Repetition period	2.4 s

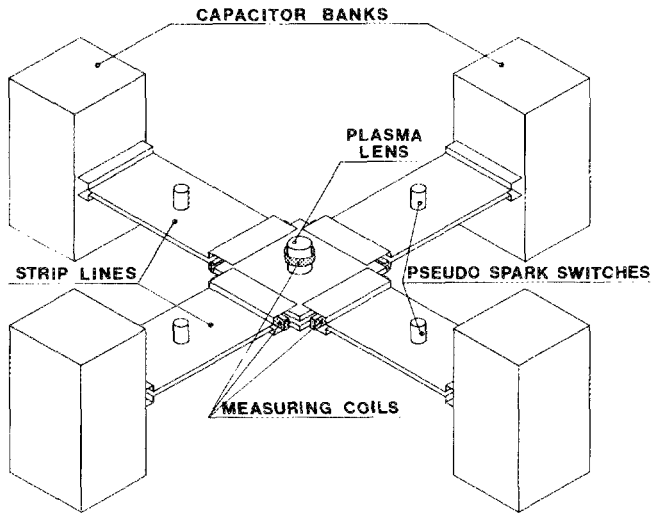

FIG. 1. Simplified block diagram of the pulse generator.

 0034-6748/87/081382-05$01.30

These considerations led to the design and construction of the differentiating measuring coils described below.

I. THEORY

The Rogowski principle[15,16] is shown in Fig. 2. For a distributed current density j which is surrounded by a closed line circumscribing an area "A," neglecting displacement currents, Oersted's law is valid

$$\oint_a \mathbf{H}\cdot d\mathbf{a} = \int\int_A \mathbf{j}\cdot d\,\mathbf{A}\,. \tag{3}$$

Integration of the right-hand term leads to

$$\oint_a \mathbf{B}\cdot d\mathbf{a} = \mu\mu_0 I\,, \tag{4}$$

where I is the total current penetrating "A." For a short line f, enclosing an area "F" by surrounding "a," the induction law can be expressed as follows:

$$\oint_f \mathbf{E}\cdot d\,\mathbf{f} = -\frac{\partial}{\partial t}\int\int_F \mathbf{B}\cdot d\,\mathbf{F}\,. \tag{5}$$

The induced voltage signal U_i is independent from the current distribution within the line "a" only under the following conditions:

(a) Stray inductance, stray capacitance, and inter-turn leakage inductance can be neglected. This is admissible only for the application in our low-frequency domain.

(b) The pick-up coil is wound n times around line a so that F always has the same area for all turns and is perpendicular to a. For a finite number of n turns, the integral in Eq. (5) can be written as a sum. The induced voltage then becomes

$$U_i = F\cdot\sum_{\nu=1}^{n}\frac{d}{dt}B_{\nu\|}\,, \tag{6}$$

where $B_{\nu\|}$ is the field component parallel to the normal vector of F.

(c) The distance Δd between turns is constant and small compared to magnetic field inhomogeneities along the integration line a. This with Eq. (4) leads to

$$\Delta d\sum_{\nu=1}^{n}B_{\nu\|} = \mu\mu_0 I\,. \tag{7}$$

For a coil length l and uniform distances Δd, the relation is

$$\Delta d = l/n\,. \tag{8}$$

Differentiating with respect to time in Eq. (7) and combined with Eq. (6) yields the induced voltage

$$U_i = \mu\mu_0 F\frac{n}{l}\frac{dI}{dt}\,. \tag{9}$$

U_i is now proportional to the time derivative of the current and the proportional factor

$$M = \mu\mu_0 F(n/l)\,,$$

contains only geometric parameters determining the sensitivity of the coil. The limit is reached when the current pulse length approaches the propagation time of the signal through the coil.

II. MEASURING CIRCUIT

The induced potential U_i is transmitted by cables of impedance Z to the monitor. Figure 3 shows the simplified circuit diagram. The symbols used in Fig. 3 are U_i is the induced signal, L_c is the coil inductance, R_c is the resistance of the coil, R is the terminating resistor, Z is the cable impedance, and U_z is the voltage on the terminating resistor.

Combining the circuit equation

$$U_i = L_c\frac{di}{dt} + (R_c + R)i\,, \tag{10}$$

with $U_z = Ri$ yields

$$U_i = \frac{L_c}{R}\frac{dU_z}{dt} + \left(\frac{R_c}{R} + 1\right)U_z\,. \tag{11}$$

As expressed by Eq. (9), U_i is proportional to the time variation of the discharge current dI/dt. Therefore, two terms of the value of $(L_c/R)\ (dU_z/dt)$ should be considered:

$$\frac{L_c}{R}\frac{dU_z}{dt} \gg \left(\frac{R_c}{R} + 1\right)U_z\,. \tag{12}$$

Here the measured signal U_z is proportional to the discharge current $\hat{I}$. The coil is self-integrating with the time constant (L_c/R).

The coils developed belong to a type, where

$$\frac{L_c}{R}\frac{dU_z}{dt} \ll \left(\frac{R_c}{R} + 1\right)U_z\,. \tag{13}$$

At this condition, U_z is proportional to dI/dt, the coil is differentiating.

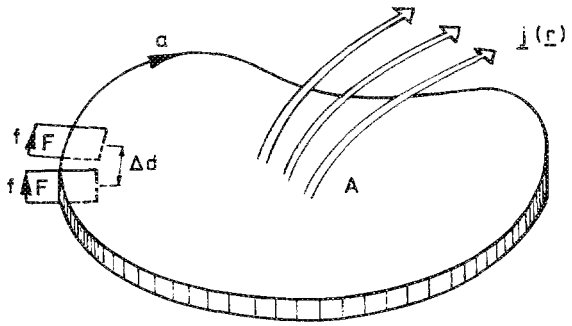

FIG. 2. Sketch of the Rogowsky principle.

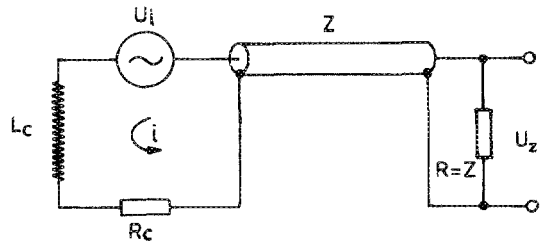

FIG. 3. Equivalent measuring circuit.

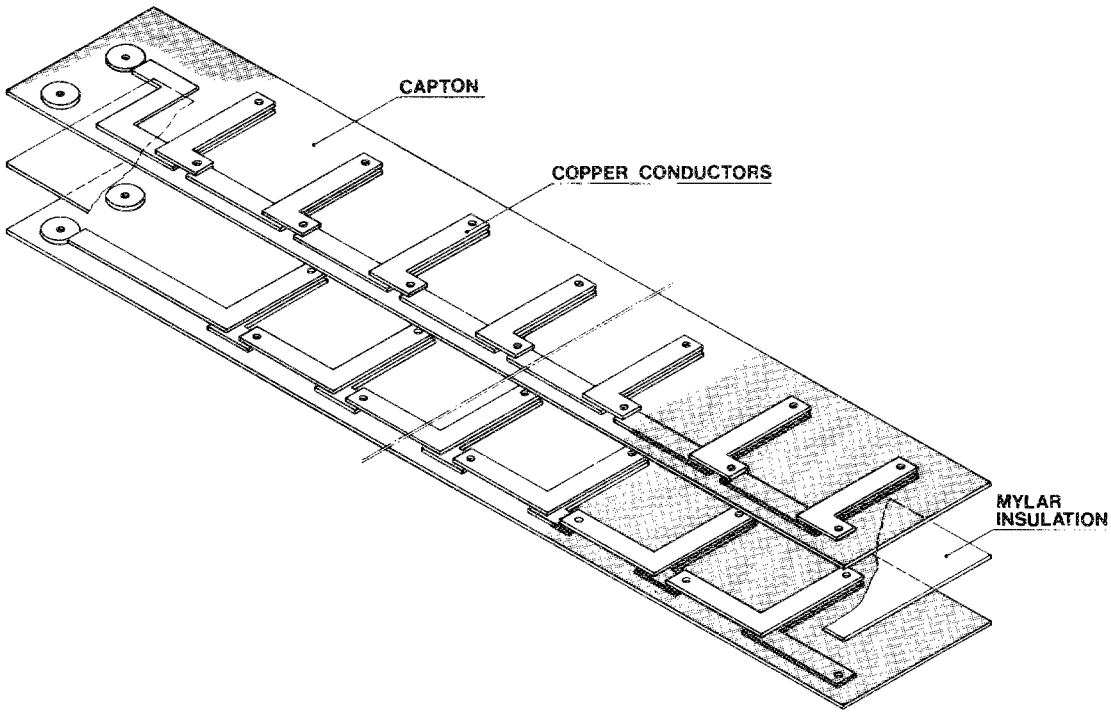

FIG. 4. The coil structure.

To evaluate Eq. (13), a harmonic approximation for U_z of

$$U_z = U_{z0} \sin \omega t \tag{14}$$

is assumed. The condition describing the upper limit for the induced frequency $\omega = \omega_{\mu l}$ of the described circuit, so that U_z is still proportional to (dI/dt), is

$$L_c \omega_{\mu l} \ll R_c + R \,. \tag{15}$$

The resistance is mainly determined by the impedance of the cable between coil and preamplifier. Thus, the self-inductance of the coil must be minimized for high-frequency transmission.

Rearranging Eq. (15) gives

$$L_c \ll (R_c + R)/\omega_{\mu l} \,. \tag{16}$$

Inserting for $R_c + R \sim 100\ \Omega$, a realistic value for a shielded twisted pair of signal cables and $2\pi \times 10^6\ \mathrm{s}^{-1}$ for $\omega_{\mu l}$, the maximal ringing frequency of the pulse generator, yields

$$L_c \ll 1.6 \times 10^{-5}\ \mathrm{H} \,. \tag{17}$$

This low inductance for a coil of 840 mm length, i.e., the circumference of the plasma cylinder, could be easily achieved by using the printed-circuit-board technique. The coils, twice 125 μm thick, have the following features:

(a) Low inductance.
(b) Greatest flatness.
(c) This extreme flatness yields high mechanical flexibility.
(d) Either the dI/dt and/or the integrated current signal can be measured.
(e) Excellent spatial integration over the current distribution.
(f) Selection of the output voltage by varying the circuit board thickness.
(g) The four-layer technique (two coils superimposed) brings the terminals to the same side. Voltage signals induced by flux penetration into the measuring coil are, therefore, suppressed.
(h) Easy reproducibility at low tolerance.
(i) Superior long-term stability.
(j) Low cost.

These considerations lead to the development of the measuring coils described.

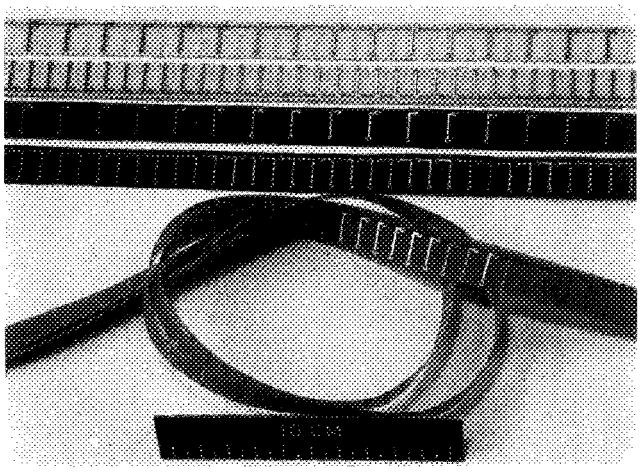

FIG. 5. Photograph of different coil types.

III. CONSTRUCTION OF THE COILS

Figure 4 shows a schematic view of the coil structure. The space available being only 20 mm between the strip lines and the central support of the plasma lens, limited the width of the coils, including the electrostatic shielding (Sec. IV).

TABLE II. Main data of the coils.

Coil No.	Number of turns (n)	Thickness (μm)	Length (mm)	Width (mm)	Winding density (cm/n)	Use
a	2×76	2×125	2×570	10	0.375	Strip line
b	2×38	2×125	2×570	10	0.75	Strip line
c	2×76	2×500	2×570	10	0.375	Strip line
d	2×38	2×500	2×570	10	0.75	Strip line
e	2×114	2×125	2×840	10	0.375	Lens
f	2×57	2×125	2×840	10	0.75	Lens

This resulted in an effective width of the turns of 10 mm. The distance of 10 mm between turns was selected to compensate for even small current displacements in the strip lines.

Introducing the necessary parameters in Eq. (9) for a selected output voltage of 100 V at a current rise of 5×10^{11} A s^{-1} and 100 cm length it follows that

$$Fn\sim1.6\times10^{-4}\ \mathrm{m}^2\ .$$

This yields a coil thickness of 160 μm at $n=100$ turns. Based on these data, different types of coils represented in Fig. 5 were constructed. The main parameters are compiled in Table II.

The winding density l/n which determines the integration step for the spatially distributed current density was selected to be either 0.750 or 0.375 cm/n. The inductance L of the coil depends only linearly and not quadratically on the length l, and therefore on n, and is determined by the strip-line geometry and can be expressed as

$$L/l=\mu_0(d/w)\ . \tag{18}$$

IV. SHIELDING

Time dependent electrical fields are present in the vicinity of the strip lines and plasma discharge and induce superimposed perturbation signals. Special care must be taken to minimize the undesired noise signals for both the strip-line coils and the plasma bobbin by using appropriate shielding.

Space restriction round the plasma lens allowed only a sandwich-type arrangement as shown in Fig. 6.

It is obvious that the thickness of the polyester film represents a compromise between minimum capacitive coupling and maximum shielding effect. It may be worth mentioning that the earthing of the copper layers is crucial.

The space available for the strip-line coils allowed to house a closed M-U shape shielding is shown in Fig. 7.

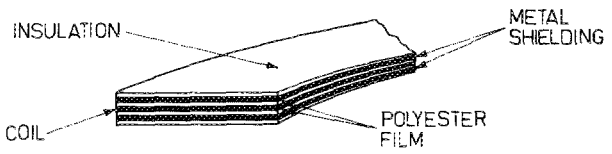

FIG. 6. Layout of an electrostatic shielding.

Several coils are accommodated in the metallic, non-magnetic case, permitting simultaneous dI/dt and $\hat{I}$ observations as well as interlock connections. The efficiency of this type of shielding is shown in Fig. 8.

V. RESULTS AND MEASUREMENTS

The results of the inductance measurements up to 5 MHz are shown in Fig. 9. All coils tested have values of less than 1000 nH and no resonant frequency was detected. Coil d was selected for the current measurements of the four strip lines and coil f was taken to monitor the current in the plasma lens.

Equation (15) gives the limit for the upper frequency $\omega_{\mu l}$, where the induced voltage U_i is still proportional to the rate of change of the current dI/dt. The measured inductance $L\sim5\times10^{-7}$ and 7×10^{-7} H for coils d and f, respectively, is more than a factor of 20 lower than stipulated in Eq. (17).

The magnetic stray field outside the strip line proved to be smaller by a factor of 40 compared to the inner field. Therefore, the measuring coils were inserted only between the plates, thus not surrounding the conductor.

Two sandwich-type shielded coils (f) surrounded the lens leading to a simultaneous $\hat{I}$ and dI/dt signal. An example of current signals is depicted in Fig. 10.

Calibration[17] up to 80 kA against a high precision, low inductive shunt shows excellent linearity and a realistic re-

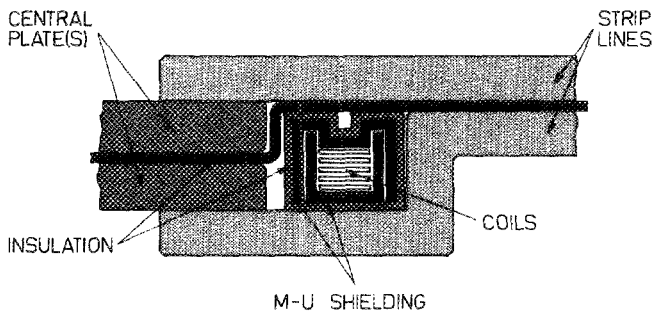

FIG. 7. Transverse cross section of coils and M-U-type shielding near central plate.

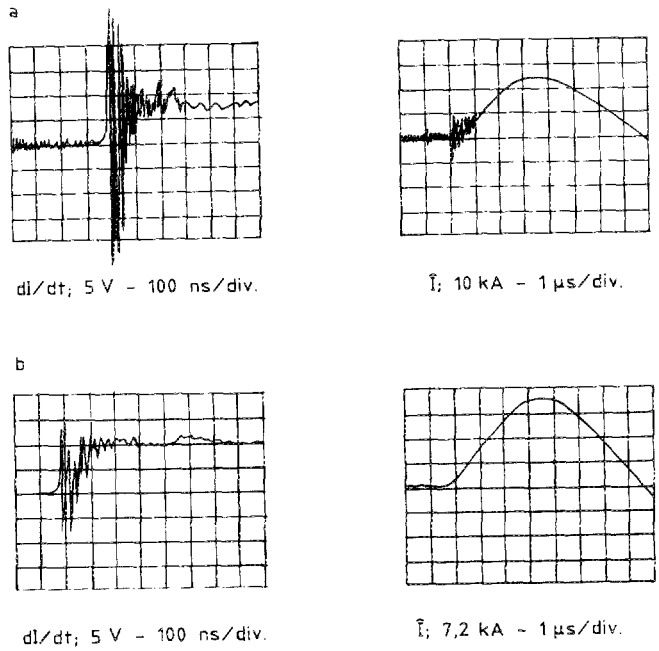

FIG. 8. Effect of shielding on noise level for: (a) sandwich-type shielding and (b) M-U-type shielding.

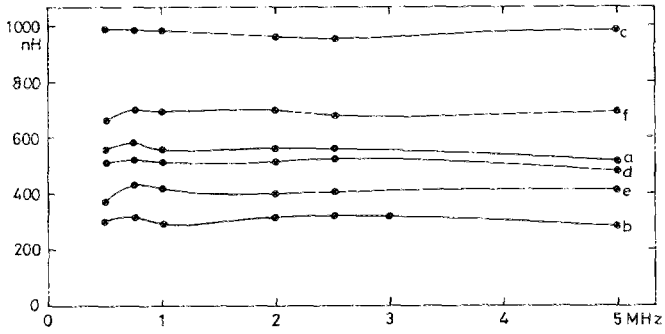

FIG. 9. Variation of self-inductance vs frequency.

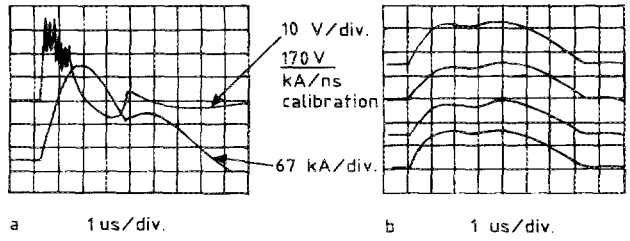

FIG. 10. Current signals of a pinched discharge: (a) $(dI/dt_{(top)})$ and $\hat{I}$; (b) simultaneous registration of the four strip-line currents (4× 100 kA).

production of the pulse shape with a passive 1-ms RC integration circuit. The ratio charging voltage/coil signal was found to be linear over the full range up to 400 kA.

VI. DISCUSSION

The common printed-circuit-board techniques allow us to reproduce from one master print, flexible multipurpose measuring coils of nearly any size.

For current pulses of higher frequencies, as in the application described, the self-inductance of the coils can be lowered by reducing the printed-circuit thickness. In addition, Eq. (9) shows that the increased dI/dt values associated with higher frequencies require a smaller geometric factor M, to reach a comparable signal amplitude. Thus, the inductance can be further reduced.

ACKNOWLEDGMENTS

The authors wish to thank their colleages H. Riege and V. Brückner for helpful conversations. This work was performed as part of CERN's ACOL Project under the leadership of E. Jones from the PS Division. The encouragement of P. Lazeyras of the Experimental Physics Facilities Division is also gratefully acknowledged.

[a] Permanent address: Physikalisches Institut der Universität Erlangen-Nürnberg, D-8520, Erlangen, Germany.
[1] L. DeMenna, G. Miano, B. Autin, E. Boggasch, K. Frank, and H. Riege, in *Proceedings of the IVth National Congress of Quantum Electronics and Plasma Physics*, Vol. 1 (1984), p. 273 and CERN/PS 84-13 (AA).
[2] E. Boggasch, H. Riege, and V. Brückner, in CERN/PS 85-30 (AA) and *Proceedings of the 5th IEEE Pulsed Power Conference*, Arlington, VA, p. III-36 (1985), pp. 820–823.
[3] C. A. Ekdahl, Rev. Sci. Instrum. **51**, 1645 (1980).
[4] J. Christiansen and C. Schultheiss, Z. Phys. A **290**, 35 (1979).
[5] D. Bloess, I. Kamber, H. Riege, G. Bittner, U. Brückner, C. Christiansen, K. Frank, W. Hartmann, N. Lieser, C. Schultheiss, R. Seebock, and W. Steudtner, Nucl. Instrum. Methods **205**, 173 (1983).
[6] G. Mechtersheimer, R. Kohler, T. Lasser, and R. Meyer, J. Phys. E **19**, 466 (1986).
[7] E. Boggasch and H. Riege, in *Proceedings of the XVIIth International Conference on Phenomena in Ionized Gases*, Vol. 2 (1985), p. 567 and CERN/PS 85-4 (AA).
[8] M. Anderson, Rev. Sci. Instrum. **42**, 915 (1971).
[9] D. G. Pellinen and P. W. Spence, Rev. Sci. Instrum. **42**, 1699 (1971).
[10] D. G. Pellinen, Rev. Sci. Instrum. **42**, 667 (1971).
[11] M. S. Di Capua, Keynote paper presented at Workshop on Measurement of Electrical Quantities in Pulse Power Systems, National Bureau of Standards, Boulder, CO, 2–4 March 1981.
[12] A. J. Schwab, *High-Voltage Measurement Techniques* (M.I.T., Cambridge, MA, 1972), pp. 163–191.
[13] D. Kind, *An Introduction to High-Voltage Experimental Technique*, 1st ed. (Vieweg, Braunschweig, Germany, 1978), pp. 50–52.
[14] G. I. Chandler and F. C. Jahoda, Rev. Sci. Instrum. **56**, Part II, 852 (1985).
[15] V. Nassisi and A. Luches, Rev. Sci. Instrum. **50**, 900 (1979).
[16] D. G. Pellinen, M. S. Di Capua, S. E. Sampayan, H. Gerbracht, and M. Wang, Rev. Sci. Instrum. **51**, 1535 (1980).
[17] A. I. Gerasimov and E. G. Dubinov, Instrum. Exp. Tech. **26**, (2), Part 2, 466 (March-April 1983).